JOURNAL OF CATALYSIS 64, 356–370 (1980)

Structure and Activity of Tellurium–Molybdenum Oxide Acrylonitrile Catalysts

J. C. J. BART[1] AND N. GIORDANO[2]

Montedison Research Laboratories, Petrochemical Division, 20021 Bollate, Milano, Italy

Received June 18, 1979

Ammoxidation of propylene to acrylonitrile (ACN) was investigated using various (Te, Mo)O catalysts at temperatures from 360 to 460°C. Binary oxides are significantly more active than the component oxides and show a completely different product distribution. The reaction leads mainly to ACN and acrolein (80–90%, in varying ratios) and to CH_3CN (3%); the balance accounts for total oxidation products. The active phase is Te_2MoO_7, which acts through activation of the hydrocarbon at Te sites and insertion of oxygen at Mo sites. Site isolation in the active phase accounts for the high selectivity to ACN. The allotriomorphic texture of Te_2MoO_7 rationalizes variations in catalytic activity of the TeO_2–MoO_3 system as a function of the composition. Decay of the catalysts by depletion of lattice oxygen was studied. Reactivation of a deactivated catalyst can be effected, but in nonequilibrium conditions transport phenomena lead to a migration of the degradation products, $TeMo_5O_{16}$, Te, and reduced molybdenum oxides. The primary function of cerium in an industrial (Ce, Mo, Te)O ammoxidation catalyst is its capacity to reoxidize its partners more readily as compared to a (Te, Mo)O solid.

INTRODUCTION

As part of the development of an industrial (Ce, Mo, Te)O catalyst for ammoxidation of propylene (*1–6*) it was felt to be of interest to consider the properties of the (Te, Mo)O system. (Te, Mo)O catalysts are very active in the oxidation of propylene ($C_3^=$) with selectivity to acrolein easily exceeding 90% (*7–9*). A characteristic feature of the system is that the ratio between the components may vary extensively without giving rise to substantial variations in catalytic activity. Evaluation of the solid-state chemistry of the (Te, Mo)O system (*10, 11*) leads to identification of Te_2MoO_7 as the active phase. Comparison with the structural features of the component oxides forms the basis for the understanding of the enhanced catalytic activity of the binary compositions.

As multicomponent (Te, Mo)O-based oxidation catalysts, especially under stream conditions, tend to suffer from the deteriorating effects of phase migration, in the form of condensates at the outlets of catalytic reactors, the solid-state relations in the reduced (Te, Mo)O system have been considered. The identification of a reduced mixed oxide $TeMo_5O_{16}$ (*11, 12*) and the knowledge of the three-phase boundaries in the reduced (Te, Mo)O system at equilibrium conditions at 550°C (*11*) have been used in a microscopic investigation of structural changes taking place under overall reducing reaction conditions. This leads to valuable information about the sequence and nature of the redox processes occurring in (Te, Mo)O-based catalysts. The results aid in the interpretation of the phenomena of aging and catalytic decay of a multicomponent industrial ammoxidation catalyst.

EXPERIMENTAL

Preparation of catalysts. (Te, Mo)O samples, including Te_2MoO_7, were prepared according to Ref. (*10*). Catalysts containing

[1] Temporary address: Department of Colour Chemistry, University of Leeds, England. Permanent address: Montedison "G. Donegani" Research Laboratories, Novara, Italy.

[2] Present address: Istituto di Chimica Industriale, Università di Messina, Messina, Italy.

0021-9517/80/080356-15$02.00/0

25 wt% active phase were obtained by standard methods, which involve mixing an acidified aqueous solution of $(NH_4)_6Mo_7O_{24} \cdot 4H_2O$ (C. Erba, 82% MoO_3) with aqueous H_6TeO_6 (Schuchardt, 98.5%). The volume of the combined solution was taken equal to the pore volume of the microspheroidal SiO_2 to be impregnated and stable salt solutions were formed over the full composition range, avoiding precipitation. After impregnation, the samples were dried at 110°C for 8 h and calcined in air at 500°C for 8 h. The industrial (Ce, Mo, Te)O ammoxidation catalyst was prepared according to the specifications of Ref. (*1*). Further reference to compositions is made in terms of molar ratios.

Testing of catalyst activity and selectivity. Catalytic activity was determined in a combined flow microreactor and gas-chromatographic unit (Fractovap Model C, C. Erba). The stainless-steel reactor (i.d. 1 cm, length 10 cm), provided with an axial thermocouple well, was heated in a coaxial oven. Precautions were taken to avoid condensation of products in the gas lines leaving the reactor and in the sampling device held at 140°C.

In a series of experiments of depletive oxidation by the slug technique, pulses of C_3H_6 and NH_3 were injected into a stream of the carrier gas (N_2) flowing through the catalyst bed held at 360°C.

In flow experiments catalytic activity results were collected under the following standard conditions: catalyst volume, 4.5 ml; feed (molar ratio) C_3H_6: NH_3: air, 1 : 1 : 10; contact time τ, 2.5 s; temperature 400–440–460°C; pressure, 1 atm. The reactants were fed into the microreactor after admixing. Results reported below refer to T = 440°C only, but in spite of this limitation they are to be considered as representative of the catalytic behavior.

Analysis of reaction products Reactants and products issuing from the reactor were analyzed by a chromatographic unit with columns (*A*), (*B*), and (*C*), operated with helium as a carrier gas. The characteristics of the chromatographic columns were as follows: (*A*) i.d. 4 mm, length 2.5 m, ethylhexyl sebacate 3% on silica; (*B*) i.d. 4 mm, length 2 m, Carbowax 1500 30% on Celite; (*C*) i.d. 4 mm, length 0.8 m, molecular sieves 5A, C. Erba. These columns achieve separation of air, CO_2, propylene, and propane at 100°C (*A*), of acetaldehyde, acetone, acrolein, acetonitrile, ACN, and H_2O at 100°C (*B*), and of CO, N_2, and O_2 at room temperature (*C*). NH_3 and HCN could not be detected by this analytical system. By allowing the carrier gas to purge a sample of the products into columns (*B*) and (*A*) separation was achieved in the order CO_2, propane, propylene; then, by excluding (*A*), acrolein, ACN, and acetonitrile. A second sample was analyzed for CO and air in column (*C*).

Propylene (C_3^-) conversion was derived from a comparison of the peak areas in the chromatograms of reactants and products. Conversions to CO, CO_2 were estimated from relative peak areas (corrected for stoichiometric and chromatographic factors) and the peak area of propylene in the feed. From the ratio of the conversions to CO, CO_2 and of C_3^- the corresponding selectivities were derived; the balance was accounted for by the selectivities to ACN, acetonitrile, and acrolein, as estimated from their peak areas corrected for all factors. Conversion (*C*) and selectivities (S_i) were defined as follows:

$$C = \frac{\text{wt } C_3^- \text{ fed} - \text{wt } C_3^- \text{ recovered}}{\text{wt } C_3^- \text{ fed}} \cdot 100\%$$

$$S_i = \frac{\text{wt } C_3^- \text{ converted to product } i}{\text{wt } C_3^- \text{ fed} - \text{wt } C_3^- \text{ recovered}} \cdot 100\%.$$

Since HCN could not be detected and other minor oxygenated products (acetaldehyde, acetone) had not been taken into account, the estimated selectivities reported are slightly overestimated. However, as quantitative runs had indicated that HCN never exceeded 2–4% yield for the most selective catalysts, with other oxygenated products being almost absent, er-

rors in the selectivities reported below are quite small.

Catalyst characterization. BET surface areas were measured using N_2 as the adsorbate. Pore volumes and pore size distribution were determined by means of a mercury porosimeter, C. Erba Models AG 60 and 70H, for the 1000- and 2000-atm range, respectively. Phase analysis was carried out by means of X-ray powder diffraction (Cu$K\alpha$ radiation, λ = 1.5418 Å). Phase distributions in the microreactor and the surface topology of catalyst grains were determined qualitatively by optical microscopy (Ortholux Leitz polarizing microscope, magnification $\sim 10^3\times$), on the basis of experience gained in the microstructural and morphological characterization of the MoO_3–TeO_2 system (*13*) and in the study of the solid-state equilibrium relations in the ternary systems MoO_3–TeO_2–MoO_2 and MoO_3–TeO_2–Te (*11*). High refractive indexes were determined using a universal stage by comparison with Merwin sulphur and selenium mixtures (*14*).

At the conclusion of activity tests in which prevailing reductive conditions were achieved during oxidation of propylene and acrolein on a SiO_2-supported Te_2MoO_7 catalyst at 360 and 420° by means of a low C_3H_6 : air ratio, the catalyst was removed from the reactor after cooling to room temperature in an N_2 atmosphere and its phase distribution was studied by optical microscopy.

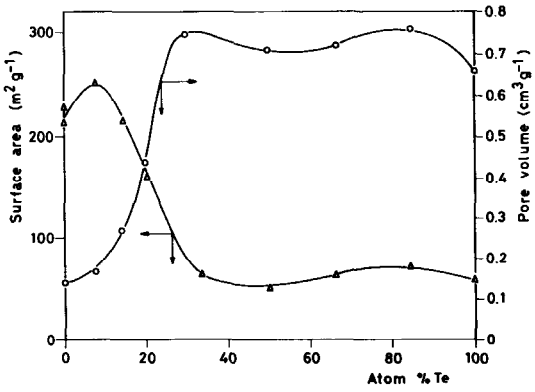

FIG. 1. Surface areas and pore volumes of SiO_2-supported TeO_2–MoO_3 catalysts calcined at 500°C for 8 h.

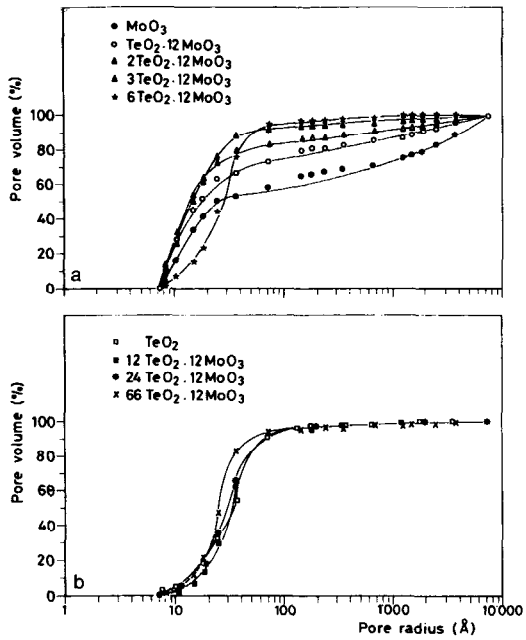

FIG. 2. *a, b* Integral distribution of the pore volume of SiO_2-supported TeO_2–MoO_3 catalysts calcined at 500°C for 8 h.

RESULTS

Morphology

Phase analysis of fresh supported catalysts indicates an amorphous or microcrystalline structure. Addition of TeO_2 to MoO_3 causes drastic effects in the morphological properties of the silica-supported system. Surface areas reach low values (50–70 m^2/g) above about 30 mole% TeO_2; correspondingly, pore volumes vary in the opposite direction (Fig. 1). Increase of tellurium thus determines a progressive rise in mean pore radius. This is in agreement with the fact that the Kelvin equation indicates that the observed variations in pore size distribution (Fig. 2) are brought about by enlargement of existing pores rather than by blocking of the smallest ones.

Catalytic Activity

Pulse experiments. Figures 3 and 4 show the effect of progressive reduction by repeatedly passing slugs of $C_3^=$ and NH_3 over SiO_2 supported (Te, Mo)O catalysts under standard conditions at 360°C. The component oxides and their interaction products differ strongly in ammoxidation activity, both with regard to $C_3^=$ conversion and the product distribution. For MoO_3-rich systems the conversion decreases sharply with oxygen depletion as opposed to the almost stationary but less active TeO_2. Assuming that equilibrium of oxidation state between surface and bulk is obtained between successive slugs, the results indicate that TeO_2 is more easily reduced than MoO_3; the latter thus contains less active oxygen atoms. On MoO_3 almost 50% of $C_3^=$ is

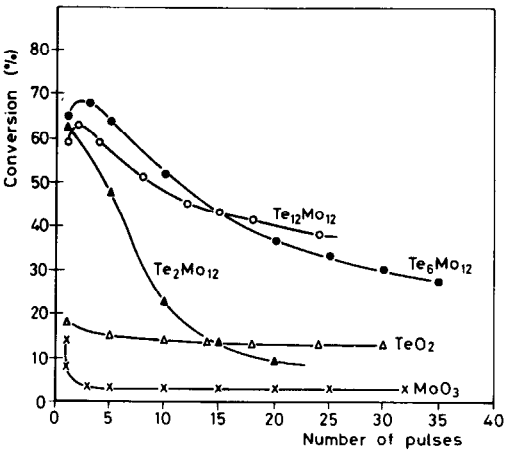

FIG. 3. Conversion of propylene in the depletive ammoxidation over SiO_2-supported (Te, Mo)O catalysts as a function of the number of pulses at 360°C under standard conditions (volume of the slug, 2 cm^3; $C_3^=$: NH_3 = 1 : 1; catalyst weight, 1.7 g; flow of carrier gas, 60 cm^3/min).

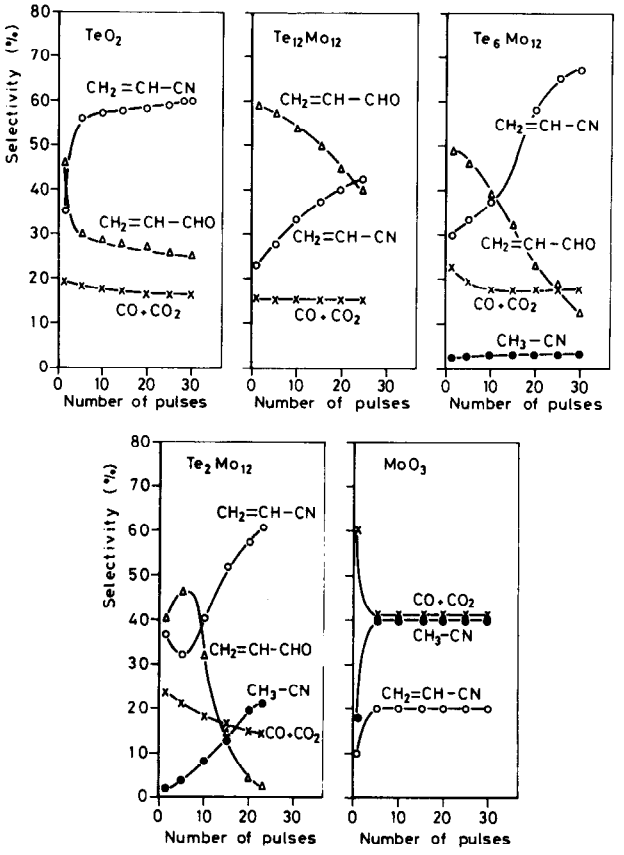

FIG. 4. Selectivities to various products in the depletive ammoxidation over SiO_2–supported (Te, Mo)O catalysts as a function of the number of pulses at 360°C under standard conditions (see Fig. 3).

converted into waste products and CH_3CN is formed as the main organic ammoxidation product (Fig. 4). TeO_2 is also quite active toward total oxidation products but ACN accounts for about 60% (Fig. 4). Interaction products of MoO_3 and TeO_2, in particular TeO_2-rich compositions, show high conversions (Fig. 3) and a combined ACN–acrolein selectivity of over 80%. The ACN fraction increases with the oxygen depletion of the catalyst, as opposed to acrolein. The amount of total waste products decreases with reduction of the catalysts, in accordance with the expectations (*15*). The by-product CH_3CN is totally absent on TeO_2-rich catalysts. In the application of (Te, Mo)O catalysts, low temperatures are conducive to formation of reductive phases and have an adverse effect on the formation of acrylonitrile. At $T <$ 300°C almost no oxidizing activity exists.

Flow experiments. Catalytic performance of the SiO_2-supported binary system MoO_3–TeO_2 at 440°C in flow conditions is given in Fig. 5. The extreme compositions exhibit an almost identical activity (65%)

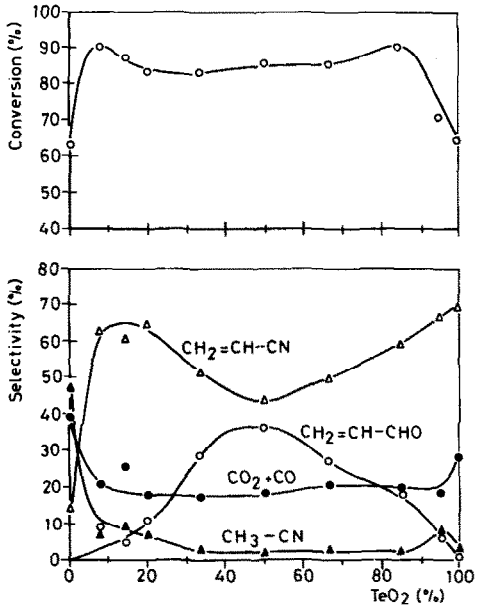

FIG. 5. Catalytic activity of SiO_2-supported (Te, Mo)O in the flow ammoxidation of propylene at 440°C (τ = 2.5 sec; C_3^- : NH_3 : air = 1 : 1 : 10).

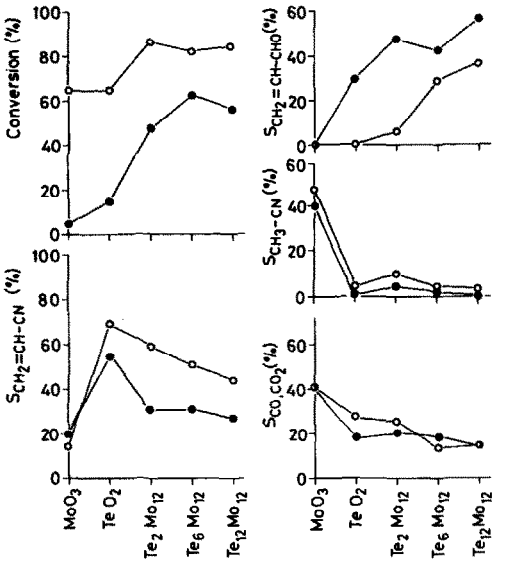

FIG. 6. Comparison between depletive (●) and flow (○) ammoxidation of propylene over SiO_2-supported (Te, Mo)O catalysts (for depletive oxidation, data taken at the fifth slug under the conditions given in Figs. 3 and 4; for flow ammoxidation, see Fig. 5).

but differ in selectivities with MoO_3 yielding mainly acetonitrile and CO, CO_2 and with TeO_2 yielding mostly ACN. Binary (Te, Mo)O compositions behave quite differently, as already noticed by Voge and Armstrong (*16*) for oxidation of propylene. The C_3^- conversion increases considerably by adding small amounts of one component to the other. In the intermediate range the conversions are rather constant.

Selectivities are more varied, with ACN increasing considerably by doping of MoO_3 with TeO_2; correspondingly, acetonitrile and carbon oxides decrease to about 3 and 20%, respectively. The selectivity to acrolein is particularly noticeable in being nil at the extremes and reaching a maximum at the molar ratio $MoO_3/TeO_2 \simeq 1$.

A comparison between pulse and flow experiments is given in Fig. 6.

Catalytic activity of Te_2MoO_7. Oxidation of propylene to acrolein using 7 cm^3 of an unsupported Te_2MoO_7 catalyst (S.A. 0.5 m^2/g, particle size 150–270 mesh) at T = 420°C (τ = 2.0 s, air: C_3^- = 14.1, vapor

TABLE 1

Catalytic Activity of Te_2MoO_7

Conversion (%)		Selectivity (%)			
Propylene	Acrolein	Acrolein	CO_2	CO	Acetaldehyde
6.5	—	91.7	8.3	—	—
—	5.7	—	53.0	8.0	39.0

40%) and of acrolein (feed: acrolein 1.8%, O_2 6%, N_2 52.2%, vapor 40%) gives results, collected at t = 6 h, as summarized in Table 1. Using a 4.5 cm^3 TeO_2:MoO = 2:1 sample (activated at 400°C for 4 h; 100–150 mesh) ammoxidation of propylene at 440°C (τ = 2.5 s, air:NH_3:C_3^- = 10.5:1.32:1) converts 46% of C_3^- (first slug) and yields 77.3% ACN, 3.4% acetonitrile, 8.0% acrolein, 8.0% CO_2, and 3.2% CO.

Reductive Degradation

The structural and textural effects on Te_2MoO_7 by oxidation of propylene and acrolein at low oxygen content in the gas feed were investigated to gain insight into the nature of the reduction processses and migration of matter (in particular tellurium), observed in pulsed microreactor experiments (cf. also (*17, 18*)). Interaction of Te_2MoO_7 with almost undiluted C_3^- at overall reducing conditions at 420°C leads to dark-blue reduction phenomena of the external surfaces of the crystallites composing the grains; at 360°C only particles at the entrance of the reactor are affected. Interaction with acrolein at 360°C leads to more extensive oxygen depletion and causes blackening at grain boundaries and internal surfaces (cleavage planes) mainly for particles at the entrance to the reactor. More homogeneous reduction along the reactor occurs at 420°C as indicated by an extensive dark-blue color. Optical examination of sliced sections reveals red-violet reflectance colors after oxidation of acrolein, typical of molybdenum in a lower than maximum valence state; the crystallite size of the reduced phases formed by interaction with acrolein exceeds that due to propylene. Net effects of birefringence and optical anisotroy at crossed nicols indicate nonisometric crystalline material; thin crystallites have green-blue absorption colors and are opaque otherwise.

Microstructural characterization shows most intense but more localized reduction at low temperature. The main differences between catalysts used for oxidation of acrolein and propylene consist in the distribution of the reduced phases. Metallic tellurium is easily detected by microchemical analysis and its high reflecting power, especially after intense reduction of the solid with acrolein at 360°C. Optical inspection shows a close genetic and topological relation to reduced binary oxide(s), as invariably the bluish-colored reduced layers on top of Te_2MoO_7 are covered with tellurium. In spite of the nonequilibrium system analyzed, the observations conform to compatibility range *b* of the phase diagram (Fig. 7).

Although MoO_3 volatilizes only above about 780°C (*19*) and requires about 55 kcal/mol (*20*), MoO_3-rich condensates were normally observed in the high-temperature regions (reaction zones) of the reactor with reduced (Te, Mo)O in colder parts next to MoO_3 and tellurium toward the outlet of the apparatus. Dark lamellar condensates were observed on grains at the top of the microreactor after oxidation of acro-

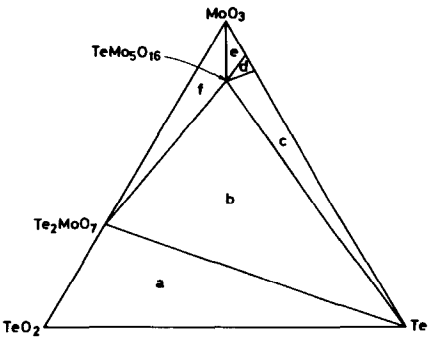

FIG. 7. Ternary phase system TeO_2–MoO_3–Te at 550°C. Compatibility ranges are: *a* = TeO_2 + Te_2MoO_7 + Te; *b* = Te_2MoO_7 + $TeMo_5O_{16}$ + Te; *c* = $TeMo_5O_{16}$ + Te + MoO_2; *d* = $TeMo_5O_{16}$ + MoO_2 + Mo_4O_{11}; *e* = $TeMo_5O_{16}$ + MoO_3 + Mo_4O_{11}; *f* = $TeMo_5O_{16}$ + Te_2MoO_7 + MoO_3.

FIG. 8. Microphotograph of a grain of a Te_2MoO_7 catalyst after reduction, showing migration of $TeMo_5O_{16}$ along reaction paths in the bulk; ×600, transparent light.

lein at 420°C. Grains sliced parallel to faces of the prismatic translucent Te_2MoO_7 crystallites showed preferred reaction paths as evidenced by reduced phases which permeate through the mass. Mobility of matter in the reactant flow is also evident from accumulation of violet condensates on top of catalyst grains in correspondence with reduction paths in the bulk (Fig. 8). In our conditions transport by intergrain contacts is negligible.

In partial agreement with our results and those of Zhiznevskii *et al.* (*18*), the oxidation of propylene at low-oxygen gas feed over Te_2MoO_7 has been reported to cause formation of Te and MoO_2 (*9, 21*).

The increase in reducibility of MoO_3 under our reaction conditions is also noticed in MoO_3-rich (Te, Mo)O systems. This is connected with the reductive degradation of Te_2MoO_7 and subsequent migration of metallic tellurium; reduction of MoO_3 crystallites sets in only in correspondence to the deposition of Te transported by the gas phase (Fig. 9). The chemical incompatibility of Te and MoO_3 is also apparent from Fig. 7 and leads to ($TeMo_5O_{16}$ + MoO_2 + Te), ($TeMo_5O_{16}$ + Mo_4O_{11} + MoO_2), or ($TeMo_5O_{16}$ + MoO_3 + Mo_4O_{11}) in equilibrium conditions depending upon the composition.

Under the conditions used for reductive degradation of (Te, Mo)O catalysts no apparent reduction phenomena are observed in (Ce, Mo, Te)O catalysts, apart from incidental blackening of some isolated grains at the entrance of the reactor (acrolein, 420°C) and no phase separation of metallic tellurium from the catalyst particles is noticed. Nevertheless, when aged, (Ce, Mo, Te)O catalysts show a tellurium gradient in the solid increasing from bulk to surface (*22*). This is in accordance with the observation that the (irreversible) migration of tellurium involves both bulk and surface (*9*).

DISCUSSION

Nature of the Active Phase

In recent years various structural models for (Te, Mo)O have been proposed (*7, 8, 10, 17, 18, 23*) and physicochemical and morphological evidence is available for Te_2MoO_7 and $TeMo_5O_{16}$ (*10–13, 24–27*). The binary compound α-Te_2MoO_7 (mp 551°C), with Te and Mo being in the (IV) and (VI) valent states, respectively, is considered by us to be the catalytically active phase in the (Te, Mo)O system. The compound is monoclinic ($P2_1/c$) with $a = 4.255_8$, $b = 8.603_6$, $c = 15.927_6$ Å, and $\beta = 95.6^\circ_1$. Dark-yellow glass (β-Te_2MoO_7) is formed by quenching of a melt of the crys-

FIG. 9. Microphotograph (×600) of a crystallite of an MoO_3 catalyst containing 5% TeO_2 showing reduction phenomena in correspondence to deposition of metallic tellurium from the gas phase.

talline α-form. The reduced (Te, Mo)O system, studied at 550°C, consists of at least six compatibility ranges, each characterized by the thermodynamic equilibrium of three phases and separated by binary phase boundaries (*11*). The coexisting phases relevant to reduction of $TeO_2 : MoO_3$ in any molar composition are (Fig. 7): (*a*) TeO_2 + Te_2MoO_7 + Te; (*b*) Te_2MoO_7 + $TeMo_5O_{16}$ + Te; (*f*) Te_2MoO_7 + $TeMo_5O_{16}$ + MoO_3. The compound $TeMo_5O_{16}$ (mp 748°C in N_2), the only reduced binary phase of the (Te, Mo)O system, is incompatible with the coexisting phases (TeO_2 + Te_2MoO_7 + Te) due to interaction with TeO_2. Above about 300°C in air $TeMo_5O_{16}$ is susceptible to oxidation to Te_2MoO_7 and MoO_3 (cf. Fig. 4 of Ref. (*11*)), according to $2TeMo_5O_{16} + O_2 \rightarrow Te_2MoO_7 + 9MoO_3$.

As salts of heteropolyacids such as $3(NH_4)_2O \cdot TeO_3 \cdot 6MoO_3 \cdot 7H_2O$ and $3(NH_4)_2O \cdot 2TeO_3 \cdot 6MoO_3 \cdot 10H_2O$ are formed by interaction of $(NH_4)_6Mo_7O_{24} \cdot 4H_2O$ and H_6TeO_6 (*28*), a substitutional solid solution $(Mo^{VI}, Te^{VI})O_3$, stereochemically possible, may eventually be formed as the first stage in the decomposition to $(Te^{IV}, Mo^{VI})O$. It is known, in fact, that thermal degradation of H_6TeO_6 to TeO_2 stabilizes TeO_3 in a suitable temperature range (*29–31*). However, as direct oxidation of TeO_2 to TeO_3 does not occur, it is less likely to form $(Mo^{VI}, Te^{VI})O_3$ starting from TeO_2, as reported by Andrushkevich *et al.* (*7*). Independent preparations of (Te, Mo)O compositions with H_6TeO_6 (*8, 10*) at $T > 450$°C invariably lead to mixtures of Te_2MoO_7, MoO_3, and/or TeO_2. The absence of Te(VI) is not surprising, since Te^{VI} is usually formed at 400–700°C in the presence of more basic cations (Al^{III}, Co^{III}, Fe^{III}, Ga^{III}, Cu^{II}, Mg^{II}, Mn^{II}, Pb^{II}, Ni^{II}, and Zn^{II}) and no such stabilization is expected in the case of molybdenum. By analogy with the system $MnO_2 \cdot Al_2O_3$ (*32*), valence change may then be invoked to rationalize formation of $(Mo^{VI}, Te^{VI})O_3$. However, this possibility is equally doubtful as TeO_3 and MoO_3 are not isomorphous, contrary to γ-Mn_2O_3 and γ-Al_2O_3. Nevertheless, let us consider the reduction of the solid solution $Te_{0.08}Mo_{0.92}O_{3.0}$. It is known that partial replacement of molybdenum in related structures occurs; in fact, such events enhance the stability of Mo_5O_{14} (*33*). However, as Ekström has pointed out (*34*), tellurium does not form $Te_{0.02}Mo_{0.98}O_{2.80}$, quite irrespective of the ionic size of the cation and its disposition to assume a pentagonal bipyramidal coordination. Therefore, the reduced $(Mo^{VI}, Te^{VI})O_3$ solid is likely to lead to stabilization of an alternative structure in the phase field near to $Te_{0.08}Mo_{0.92}O_{3.0-x}$. It appears that $Te_{0.16}Mo_{0.84}O_{2.67}$ or $TeMo_5O_{16}$ is a quite acceptable solution. It is obvious then that $(Mo^{VI}, Te^{VI})O_3$ is not to be considered as a stable oxidation catalyst as reduction leads to a system which upon reoxidation yields $(Mo^{VI}, Te^{IV})O$. It is likely that this holds true also for $MoO_3 \cdot TeO_3$-based catalysts (*35*).

It is finally to be mentioned that $(Mo^{VI}, Te^{IV})O_{3-x}$ solid solutions have not been reported although their formation has been suggested (*17*). Similarly, stabilization of the MoO_2 rutile structure in the TeO_2 pseudorutile lattice (*23*) lacks experimental evidence.

Structure and Activity

Catalytic activity. The general character of the results depends upon the preparative route, Te/Mo ratio, and reaction conditions. Table 2 compares reported conditions for catalytic (amm)oxidation over (Te, Mo)O systems. According to Arnaud *et al.* (*9*) samples in the ranges Te/Mo = 1/9–0 and 2–9 show high critical temperatures for achieving standard conversions. Selectivity to acrolein is high (>95%) in the intermediate composition range but lower at the extremes. Using catalysts prepared by activation of H_6TeO_6 and $(NH_4)_6Mo_7O_{24} \cdot 4H_2O$ at low temperatures (*18*), the selectivity to methacrolein at 400°C is fairly constant over the whole composition range (90%) but drops to 40% for MoO_3; conver-

TABLE 2

Catalytic Oxidation over (Te, Mo)O Systems

Catalyst Preparation		Phase distribution	Reagents	Reaction conditions		Ref.
Starting materials	Activation			Reaction mixture	T°(C)	
H_6TeO_6,$(NH_4)_6Mo_7O_{24}\cdot 4H_2O$	500°C, 18 h	TeO_2,MoO_3,Te_2MoO_7	Propylene	C_3^-:air = 1:10 C_3^-:N_2 = 1:10	440–530° 500°	*9*
H_6TeO_6,$(NH_4)_6Mo_7O_{24}\cdot 4H_2O$	500°C[d]	[Te/Mo = 1:1]	Propylene	C_3^-:O_2 = 1:1.8	400–500°	*50*
TeO_2,$(NH_4)_6Mo_7O_{24}\cdot 4H_2O$	430°C, 7 h	TeO_2,MoO_3,$[TeMo_5O_{16}]$[a], $(Mo^{VI},Te^{VI})O_3$	Propylene	C_3^-:O_2 = 1:7	390°	*7*
TeO_2,MoO_3,(MoO_2),SiO_2	420°C, 4 h	not given	Propylene	C_3^-:O_2 = 1:1.5	375–450°	*16*
H_6TeO_6,$(NH_4)_6Mo_7O_{24}\cdot 4H_2O$	500°C, 8 h	Te_2MoO_7	Propylene, acrolein	C_3^-:air = 1:14	360, 420°	This work
$MoTe_2$	650°C, 16 h	$MoTe_{1.8}O_{4.9}$[b]	Propylene, isobutene	C_n^-:O_2 = 0.5–2.0	400–475°	*51*
H_6TeO_6,$(NH_4)_6Mo_7O_{24}\cdot 4H_2O$	400°C, 8 h	TeO_2,Te,MoO_3,MoO_2, $[TeMo_5O_{16}]$[a,c]	isobutene	C_4^-:O_2 = 1:1	400°	*18*
TeO_2,MoO_3	not given	not given	NH_3	NH_3:air = 1.11	not given	*23*
H_6TeO_6,MoO_3;$(NH_4)_6TeMo_6O_{24}\cdot 7H_2O$,$SiO_2$	420°C	$TeO_3.6MoO_3$[c]	Propylene	C_3^-:O_2:H_2O = 1:1:6	455–490°	*35*
H_6TeO_6,$(NH_4)_6Mo_7O_{24}\cdot 4H_2O$,$SiO_2$	500°C, 8 h	TeO_2,MoO_3,Te_2MoO_7	Propylene, NH_3	C_3^-:NH_3:air = 1:1:10	440°	This work
TeO_2,MoO_3,SiO_2	400°C, 4 h	not given	Propylene, NH_3	C_3^-:NH_3:O_2 = 1:1:2	440°	*53*

[a] Supposed on the basis of reported data.
[b] Probably a mixture of Te_2MoO_7, $TeMo_5O_{16}$ and MoO_3 (*52*).
[c] Phase distribution determined after testing the catalytic activity.
[d] Not specified.
[e] Empirical composition.

sion of isobutene is maximum at about 70 at.% Mo. A similar selectivity–composition relationship is found by Andrushkevich *et al.* (*7*) in the oxidation of C_3^- at 390°C with maximum activity at $TeO_2/MoO_3 = 0.08$. TeO_2 is inactive at 390°C whereas MoO_3 converts 8% of C_3H_6 to 50% total oxidation products and 35% acrolein ($\tau = 35$ s). Low ammoxidation activity of MoO_3 has also been reported by Gel'bshtein *et al.* (*36*).

Figure 5 shows maximum activity and high ACN selectivity over a wide range of binary compositions with the component oxides being much less active. Comparison of (Te, Mo)O with other systems, such as (Bi, Mo)O and (U, Sb)O, shows similar synergetic effects by combination of two different cations in a suitable configuration. As commonly found, in ammoxidation catalysis the C_3^- conversion into waste products is less than in the oxidation process (without NH_3), indicating that NH_3 inhibits the destructive oxidation of propylene.

The observed variations in the rates of the main and side reactions in the process of ACN formation are rationalized by the change in catalyst surface properties. Partial reduction of the surface of TeO_2 and (Te, Mo)O catalysts (as opposed to MoO_3) apparently does not greatly alter the active oxygen distribution in the surface layers of the lattice, as the total selectivity to partial oxidation products remains constant.

The increase in ACN yield with reduction of the catalysts apparently contrasts with the proposed mechanism of ammoxidation of propylene over cerium-doped bismuth molybdate catalysts which indicates Mo^{VI} active sites for ACN formation (*37*). However, in agreement with the concepts of Callahan and Grasselli (*15*), oxygen depletion leads to a less favorable active oxygen topology for the highly oxygen-demanding total oxidation, thus favoring more selective processes. Clearly, this simple picture may require amendments if oxygen diffusion processes are to be taken into account. The opposed trends of ACN and acrolein as the reaction proceeds and the practically identical reaction rates of oxidation and oxidative ammonolysis also suggest that acrolein could be a minor intermediate in the formation of ACN, in accordance with earlier suggestions (*36*). It is of interest to notice that acrolein is a trace product on (Bi, Mo)O and (U, Sb)O.

According to Zhiznevskii *et al.* (*18*), apart from TeO_2, oxidation of isobutene over (Te, Mo)O catalysts at 360°C proceeds chiefly by an associative reaction between the olefin and oxygen adsorbed by the catalyst surface rather than by the stepwise oxidation–reduction scheme of (Bi, Mo)O, (Co, Mo)O, (Fe, Sb)O, and (Sn, Sb)O catalysts (*38*). However, at slightly higher temperatures (390–410°C) oxidation over (Te, Mo)O also takes place by the redox mechanism (*7*) and only a certain contribution to CO_2 formation can be ascribed to the associative mechanism. Similarly, at 500°C selective oxidation of C_3^- to acrolein proceeds by reduction of the (Te, Mo)O lattice followed by reoxidation of the oxygen-depleted catalyst by interaction with gaseous oxygen (*9*).

Consideration of the usual reaction mechanism (involving allylic oxidation), in conjunction with the inorganic chemistry of the catalyst, allows tentative identification of the site of adsorption. Since Te^{4+} can π-adsorb olefins (cf. oxidation activity of TeO_2), it seems reasonable to suggest that adsorption centers about this ion, with electron transfer to molybdenum ions.
Schematically:

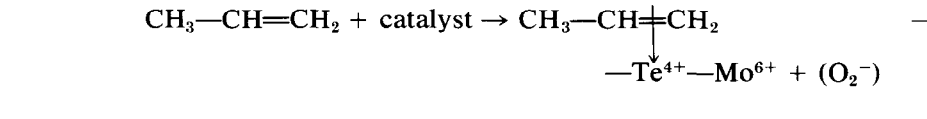

$$CH_2{=}CH{=}CH_2^- \rightarrow CH_2{=}CH{=}CH_2$$
$$\downarrow \qquad\qquad\qquad \downarrow$$
$$-Te^{4+}-Mo^{6+} + (O_2H) \qquad -Te^{4+}-Mo^{5+} + (O_2H)$$

The similarity of the results in flow experiments at 440°C with O_2 and slug experiments at 360°C without O_2 (Fig. 6) clearly confirms the role of lattice oxygen in the reaction. After the rate-determining step of π-allyl adsorption of the olefin with abstraction of hydrogen, removal of oxygen atoms from distorted molybdenum octahedra is facilitated by the fact that the bond strengths vary over a wider range than in the case of tetrahedral or trigonal bipyramidal M–O structures (*e.g.*, oxo–Te^{IV} environments). Bond valence values in Te_2MoO_7 vary from 0.15 to 1.8 v.u. for Mo–O and from 0.5 to 1.2 v.u. for Te–O, against 0.3–2.0 v.u. in MoO_3 (*39*). Not surprisingly, therefore, Andrushkevich *et al.* (*7*) ascribed the change in catalytic properties of MoO_3 on introduction of tellurium to the influence of this cation on the bond energy of the oxygens taking place in the oxidation. However, according to Grzybowska, Haber, and Janas (*40*), the main reason for the poor performance of MoO_3 lies in its inability to activate the hydrocarbon.

Noteworthy is the selectivity of acrolein, especially for tellurium-rich (Te, Mo)O catalysts and TeO_2. Acrolein formation is highest with fully oxidized (Te, Mo)O catalysts and drops sharply with reduction. Production of waste products is low for the fully oxidized state and decreases with reduction. Yet, selectivities to CO, CO_2 exceed those to acrolein beyond certain reduction levels (higher for tellurium-rich binary oxides), suggesting that there are actually two types of lattice oxygen involved in the ammoxidation over (Te, Mo)O. One type of oxygen is primarily active in selective oxidation, the other in producing waste products. As the former are most easily depleted they are less numerous and probably the less tightly bound.

The enhanced activity is in accordance with the fact that introduction in the lattice of an *n*-type oxide (d^0 cations) of low-lying accepter levels (reducible cations) lowers the Fermi level (and *n*-type character) and raises the work function (*41*); the reducibility increases and consequently the overall activity. In a different view, the increased reducibility is on account of stabilization of a well-defined intermediate valence state as a result of the very high electronegativity of tellurium (*42*). In this respect, it is noteworthy that other often used variable valence state cations in ammoxidation processes (Sb, Sn) also have high electronegativity values. The greater reducibility of Te_2MoO_7 than MoO_3 is also clearly seen from the compatibility range *f* in the TeO_2–MoO_3–Te phase diagram (Fig. 7), where MoO_3 coexists together with reduced molybdenum chemically combined to tellurium in the binary oxide $TeMo_5O_{16}$.

It is noticed that Mo^V ions are already formed after evacuation of (Te, Mo)O solids at 350°C or higher or after treatment with a reaction mixture (C_3H_6 + O_2) at 380°C (*43*). The appearance of tellurium at the (sub)surface, along with stabilization of the Mo^V ions, promotes structural changes under the reaction conditions. Blocking of the MoO_3 surface by Te_2MoO_7 and TeO_2 with increasing Te contents leads to a decrease in Mo^V ions. Other paramagnetic centers, resulting from abstraction of weakly bonded surface oxygen followed by redistribution of the Mo^V bond valences to form a square-pyramidal structure with approximate C_{4v} symmetry and bond orders of 0.75(4x) and 2.0 v.u., appear at 550°C for Te/Mo > 0.5 and increase sharply toward higher Te contents (*43*). Similar EPR signals are found in partially reduced $MoO_3 \cdot SiO_2$ and (Bi, Mo)O catalysts (*44, 45*).

Oxygen replenishment probably occurs by transfer of O^{2-} from the environment of

Te to that of Mo followed by reoxidation of Te. Schematically:

$$2Mo^{5+} + Te^{4+} \rightarrow 2Mo^{6+} + Te^{2+} \xrightarrow{ox.} Te^{4+}.$$

(Eventually Te^{3+} may be visualized, but Te^{2+} is preferred here as it is known to give relatively stable complexes (*46*)). Details concerning reoxidation of the oxygen-depleted catalytic system (Te, Mo)O are not available, in contrast to the case of partially reduced MoO_3 (*47*). By analogy with this system, a substantial difference may be expected between the properties of the surface pentavalent molybdenum ions in the composition of Te_2MoO_7 and those deposited on silica gel (cf. MoO_3 and $MoO_3 \cdot SiO_2$ (*44*). The observation that the catalyst tends to degrade in the absence of oxygen leads to the conclusion that the passage of O^{2-} from Te to Mo might lead to decomposition unless reduced Te is quickly regenerated by interaction with O_2.

Nature of the active sites Higher mobility and accessibility to gaseous reactants of three tellurium-bound oxygens of Te_2MoO_7 has been invoked (*9*) to explain the greater catalytic activity of this compound as compared to MoO_3, with reduction of tellurium both at the surface and in the bulk. However, from a structural point of view, α-Te_2MoO_7 should not be regarded as having preferred reaction paths in the form of pores or tunnels, comparable to, *e.g.*, Mo_5O_{14}. Namely, the structure consists of a close-packing arrangement of oxygen atoms and tellurium lone pairs (*25*). Therefore, we feel that the more critical differences between Te_2MoO_7 and MoO_3 with respect to oxidation catalysis are: (i) Mo^{VI} site isolation in Te_2MoO_7 as opposed to the regular array of such cations in the layer structure of MoO_3; (ii) lower bond strengths of weakest Mo–O bonds in Te_2MoO_7; (iii) the allotriomorphic nature of Te_2MoO_7 as compared to the idiomorphic MoO_3; (iv) the olefin-activating properties of Te^{4+} cations.

Te_2MoO_7 appears as a typical example of a compound where application of the topochemical site isolation concept (*15*) explains the high selectivity for (amm)oxidation of propylene. This can be seen by comparison of the crystal structures of α-Te_2MoO_7 (*25*) and MoO_3 (*48*). The former is composed of (1 × 2) blocks of edge-sharing, symmetry-related molybdenum octahedra, forming $[Mo_2O_{10}]^{8-}$ units polymerized to $[Mo_2O_8]_n^{4n-}$ stacks linked by corner sharing to puckered $[Te_2O_6]_n^{4n-}$ strings. MoO_3 has a typical layer structure and thus provides a completely different distribution of active oxygen atoms. As the building blocks and metal–oxide bond energies in Te_2MoO_7 are essentially those of TeO_2 (trigonal bipyramids) and MoO_3 (octahedra), it follows that Te_2MoO_7 contains active oxygens in a field of less active atoms. If we assume that the rate of diffusion from bulk to surface is slow relative to contact times, then the overall higher level of selectivity to CO, CO_2 on MoO_3 indicates a more favorable geometry for total oxidation than on Te_2MoO_7, in agreement with the expectations based on the layer-type structure. Instead, the increased site isolation in Te_2MoO_7 compared to MoO_3 determines a beneficial effect on the selective heterogeneous catalytic (amm)oxidation of propylene. The improved conversion is related primarily to the activation of propylene on Te sites and further to the lower bond strength of the weakest Mo–O bonds in Te_2MoO_7 (2.534 Å, 0.17 v.u.) as compared to MoO_3 (2.332 Å, 0.28 v.u.), as also expressed by the difference in ⟨Mo–O⟩ lengths, namely, 1.996_6 and 1.980_8 Å, respectively.

Morphology of the active phase. On the basis of the nature of the active phase, catalytic activity might be expected to vary linearly with the phase distribution according to the phase diagram TeO_2–MoO_3. However, at first sight the conversion of propylene at 440°C in the ammoxidation reaction (Fig. 5) is suggestive of doping in the (Te, Mo)O system rather than compound formation. In order to explain this anomaly, textural changes accompanying chemical interaction in the (Te, Mo) system

should be taken into account. The allotriomorphic solid Te_2MoO_7 has been shown to act as an interparticle ligand. As a result of this cementing function the catalytic activity of TeO_2–MoO_3 binary mixtures is very similar to that of the pure phase Te_2MoO_7, as observed. The (Te, Mo)O system thus presents typical features of "adlineation" promotion (*13*).

Decay of catalytic activity. An important difference between the ammoxidation catalysts (Bi, Mo)O, (U, Sb)O, and (Te, Mo)O lies in the sensitivity to reduction. (Bi, Mo)O can be reduced to a considerable extent without losing its properties, due to fast diffusion through the bulk. Instead, in (U, Sb)O catalysts mainly surface oxygen ions are involved in the process, leading to a great sensitivity to reduction and easy decomposition of the system. In (Te, Mo)O solids migration of reduced phases is a limiting factor in technical application (*16*).

(Te, Mo)O catalysts can be reduced to a considerable extent by the olefin in the absence of oxygen sometimes even with a positive effect on the oxidation properties in certain reaction conditions (*17*). If we consider that the promotional effect of tellurium on molybdenum consists in establishing conditions of higher reducibility of the catalyst toward olefins, then the (Te, Mo)O system is only catalytically stable if the reoxidation rate can be made to balance the increased reduction rate. This is not always achieved in practice and slow reoxidation ($k_{ox} < k_{red}$) occurs frequently. Although no thorough study of the oxidation–reduction rates of (Te, Mo)O has been made, $k_{ox} \approx 4k_{red}$ at 360°C (*18*). Therefore, during reduction at this temperature oxygen diffusion to the surface is not a limiting stage. Reduced molybdenum oxides are often reoxidized with some difficulty, especially at low temperature. In certain instances (*49*), full reoxidation of depleted molybdenum oxide is accomplished only at $T \approx 500$°C.

In overall reducing conditions or at inherently slow oxygen diffusion in the catalyst, degradation processes lead to reduced phases, among which Te and MoO_x ($2 \leq x < 3$). This follows from the coverage of Te_2MoO_7 grains with layers of a dark-blue compound and Te and by phenomena of pseudomorphism. Lamellar cogrowth of Te and molybdenum oxides in the habit of reduced (Te, Mo)O crystallites has been observed in reactor condensates. As to the nature of other reduced phases, $TeMo_5O_{16}$ is strongly indicated and also appears in Russian work (*7, 17, 18*). Namely, the unknown phase *X* in the (Te, Mo)O system of Andrushkevich *et al.* (*7*), characterized by sparse X-ray data (d = 3.96, 3.35, 3.05, 2.92, 2.57 Å), is either Te_2MoO_7 (d = 3.78, 3.32, 3.04, 2.91, 2.89, 2.63 Å) or, in view of its preferential formation in reducing medium, $TeMo_5O_{16}$ (d = 4.07, 3.34, 2.93 Å). Whereas the former is active, the latter compound apparently has low selective oxidizing power in the reaction with propylene (*7*). This is probably related to the absence of propylene activating centers, the fairly regular array of MoO_6 octahedra in $TeMo_5O_{16}$ and the more strongly bonded oxygens. Further, as is well known, selective ammoxidation requires Mo^{VI} sites whereas Mo^{V} sites are responsible for HCN, acetonitrile, CO and CO_2 (*37*). However, the phase *I* of Fedevich *et al.* (*17*) (d = 4.0, 3.35, 3.32, 2.90, 2.59, 2.41, 2.04, 1.75, and 1.73 Å), present in a partially reduced (Te, Mo)O catalyst (to 6%), is also identified by us with $TeMo_5O_{16}$; nevertheless, this catalyst shows considerable oxidation activity toward isobutene at 340°C.

Flow conditions in the reactor are particularly favorable for reduction to cause structural and textural changes. Formation of reduced (Te, Mo)O and metallic tellurium from Te_2MoO_7 (cf. compatibility range *b* in Fig. 7), phase separation from the grains, migration with the reactant gas mixture, and chemical interactions after deposition (*e.g.*, further reduction of $TeMo_5O_{16}$ to Te and MoO_2 or interaction of Te with the support) are responsible for the tellurium gradient and phase distribution ob-

served in pulsed microreactor experiments using (Te, Mo)O-based oxidation catalysts. Obviously, once phase separation of the components of the oxidation catalyst has occurred, the initial composition and original catalytic activity can no longer be restored by reoxidation.

Oxygen regeneration may be achieved either by modification of the experimental conditions (*e.g.*, higher reaction temperature, insofar as compatible with the requirements of catalytic activity and selectivity; cf. also Fig. 4 of Ref. (*11*)) or by introduction of other active elements. For the catalytic ammoxidation of propylene to ACN a steady state involving matching of the redox rates has been achieved in (Ce, Mo, Te)O solids (*1*). The third component counteracts the reductive degradation of the (Te, Mo)O subsystem by its high reoxidation capacity ($k_{ox} \geq k_{red}$). Details of this industrial catalyst are given in papers by Caporali (*4–6*).

CONCLUSIONS

Experimental evidence supports the view that selective heterogeneous oxidation of propylene to acrylonitrile over (Te, Mo)O solids is catalyzed by Te_2MoO_7. The high catalytic activity is explained by activation of propylene on Te sites and oxygen insertion at isolated and highly distorted MoO_6 octahedral sites. Instability of (Te, Mo)O-based catalysts derives from migration of reduced phases due to transport phenomena but the reductive degradation of Te_2MoO_7 is suppressed in (Ce, Mo, Te)O catalysts.

ACKNOWLEDGMENTS

One of us (J.C.J.B.) is indebted to Montedison S.p.A. (R. & D. Division) for a leave of absence and to the Ramsay Memorial Trust (London) for financial assistance. Thanks are due to Dr. A. Marzi (Bollate) for preparation of the microphotographs.

REFERENCES

1. Caporali, G., Ferlazzo, N., and Giordano, N. (to Montecatini-Edison), U.S. Patent 3,691,224 (Sept. 12, 1972).
2. Caporali, G., Ferlazzo, N., and Giordano, N. (to Montecatini-Edison), Italian Patent 820,619 (Aug. 1, 1968).
3. Cevidalli, G,, Nenz, A., and Caporali, G., *Chim. Ind. Milan* **49**, 809 (1967).
4. Caporali, G., *AIChE Symp. Ser.* **69**, 92 (1972).
5. Caporali, G., *Hydrocarbon Process.* **51**, 144 (1972).
6. Caporali, G., *Chim. Ind. Milan* **59**, 367 (1977).
7. Andrushkevich, T. V., Boreskov, G. K., Kuznetsova, L. L., Plyasova, L. M., Tyurin, Y. N., and Shchekochikhin, Y. M., *Kinet. Katal.* **15**, 424 (1974).
8. Robin, J. Y., Arnaud, Y., Guidot, J., and Germain, J. E., *C.R. Acad. Sci. Ser. C* **280**, 921 (1975).
9. Arnaud, Y., Guidot, J., Robin, J. Y., Romand, M., and Germain, J. E., *J. Chim. Phys.* **73**, 651 (1976).
10. Bart, J. C. J., Petrini, G., and Giordano, N., *Z. Anorg. Allg. Chem.* **412**, 258 (1975).
11. Bart, J. C. J., Petrini, G., and Giordano, N., *Z. Anorg. Allg. Chem.* **413**, 180 (1975).
12. Arnaud, Y. and Guidot, J., *Acta Crystallogr.* **B33**, 2151 (1977).
13. Bart, J. C. J., Marzi, A., Pignataro, F., Castellan, A., and Giordano, N., *J. Mater. Sci.* **10**, 1029 (1975).
14. Merwin, H. E., and Larsen, E. S., *Amer. J. Sci.* **34**, 42 (1912).
15. Callahan, J. L., and Grasselli, R. K., *AIChE J.* **9**, 755 (1963).
16. Voge, H. H., and Armstrong, W. E. (to Shell), French Patent 1,342,963 (Oct. 4, 1962).
17. Fedevich, E. V., Zhiznevskii, V. M., Nikipanchuk, M. V., Yakubovskaya, L. F., and Golub, I. M., *Kinet. Katal.* **15**, 1288 (1974).
18. Zhiznevskii, V. M., Fedevich, E. V., Pikulyk, O. M., Shipailo, V. Y., and Tolopko, D. K., *Kinet. Katal.* **13**, 1488 (1972).
19. Dupuis, T., *Mikrochem. Mikrochim. Acta* **35**, 449 (1950).
20. Pozin, M. E., Ginstling, A. M., and Pechkovskii, V. V., *Zh. Prikl. Khim.* **27**, 273 (1954).
21. Arnaud, Y., and Guidot, J., *C.R. Acad. Sci. Ser. C* **282**, 631 (1976).
22. Bart, J. C. J., Castellan, A., and Giordano, N., unpublished results.
23. Schulz, I. W., and Scheve, J., "*Symposium on the Mechanisms of Hydrocarbon Reactions,*" Siófok, 5–7 June 1973, p. 28.
24. Petrini, G., Bart, J. C. J., Perissinoto, P., and Giordano, N., "Proc. 4th ICTA," Budapest, 8–13 July 1974, Vol. 1, p. 387.
25. Bart, J. C. J., and Giordano, N., *Gazz. Chim. Ital.* **109**, 73 (1979).
26. Arnaud, Y., Averbuch-Pouchot, M. T., Durif, A., and Guidot, J., *Acta Crystallogr.* **B32**, 1417 (1976).

27. Bart, J. C. J., unpublished results.
28. Meloche, V. W., and Woodstock, W., *J. Amer. Chem. Soc.* **51,** 171 (1929).
29. Rosický, J., Loub, J., and Pavel, J., *Z. Anorg. Allg. Chem.* **334,** 312 (1965).
30. Bayer, G., *Fortschr. Mineral.* **46,** 41 (1969).
31. Bart, J. C. J., Bossi, A., Castellan, A., Perissinoto, P., and Giordano, N., *J. Therm. Anal.* **8,** 313 (1975).
32. Selwood, P. W., Moore, T. E., Ellis, M., and Wethington, K., *J. Amer. Chem. Soc.* **71,** 693 (1949).
33. Kihlborg, L., *Acta Chem. Scand.* **23,** 1834 (1969).
34. Ekström, T., *Chem. Commun. Univ. Stockholm,* No. 7 (1075).
35. Fetterley, L. C. (to Shell), Belgium Patent 623,610 (April 16, 1963).
36. Gel'bshtein, A. I., Stroeva, S. S., Kulkova, N. V., Bakshi, Y. M., Lapidus, V. L., Vasil'eva, I. B., and Sevast'yanov, N. G., *Neftekhimiya 4,* 906 (1964).
37. Giordano, N. and Bart, J. C. J., *Rec. Trav. Chim. Pays Bas* **94,** 28 (1975).
38. Parfenov, A. N., Dumin, D. A., Stroeva, S. S., and Gel'bshtein, A. I., *Kinet. Katal.* **11,** 935 (1970).
39. Brown, I. D., and Wu, K. K., *Acta Crystallogr.* **B32,** 1957 (1976).
40. Grzybowska, B., Haber, J., and Janas, J., *J., Catal.* **49,** 150 (1977).
41. Germain, J. E., *Intra-Sci. Chem. Rep.* **6,** 101 (1972).
42. Maksimovskaya, R. I., Anufrienko, V. F., and Kolovertnov, G. D., *Kinet. Katal.* **9,** 1186 (1968).
43. Maksimov, N. G., Andrushkevich, T. V., Tyurin, Y. N., and Anufrienko, V. F., *Kinet. Katal.* **15,** 472 (1974).
44. Vorotyntsev, V. M., Shvets, V. A., and Kazanskii, V. B., *Kinet. Katal.* **12,** 1249 (1971).
45. Burlamacchi, L., Martini, G., and Ferroni, E., *Chem. Phys. Lett.* **9,** 420 (1971).
46. Foss, O., *in* "Selected Topics in Structure Chemistry" (P. Andersen, O. Batiansen, and S. Furberg, Eds.), p. 145. Universitetsforlaget, Oslo, 1967.
47. Cornaz, P. F., Van Hooff, J. H. C., Pluym, F. J., and Schuit, G. C. A., *Discuss. Faraday Soc.* **41,** 290 (1966).
48. Kihlborg, L., *Ark. Kemi* **21,** 357 (1963).
49. Mosesman, M. A., *J. Phys. Chem.* **73,** 5635 (1951).
50. Robin, J. Y., and Germain, J. E., *Bull. Soc. Chim. Fr.,* 1511 (1976).
51. Ondrey, J. A. and Swift, H. E. (to Gulf), U.S. Patent 3,641,138 (Feb. 8, 1972).
52. Bart, J. C. J., Van Truong, N., Antonucci, P., and Giordano, N., unpublished results.
53. Minekawa, S., Hoshino, S., Shibata, A. and Kominami, N. (to Asahi), U.S. Patent 3,164,626 (Jan. 5, 1965).